J Appl Electrochem (2007) 37:1439–1446
DOI 10.1007/s10800-007-9349-6

ORIGINAL PAPER

Electroreduction of oxygen at tungsten oxide modified carbon-supported $RuSe_x$ nanoparticles

P. J. Kulesza · K. Miecznikowski · B. Baranowska · M. Skunik · A. Kolary-Zurowska · A. Lewera · K. Karnicka · M. Chojak · I. Rutkowska · S. Fiechter · P. Bogdanoff · I. Dorbandt · G. Zehl · R. Hiesgen · E. Dirk · K. S. Nagabhushana · H. Boennemann

Received: 26 February 2007 / Revised: 11 June 2007 / Accepted: 11 June 2007 / Published online: 3 July 2007

Abstract WO_3-modified carbon-supported bi-component ruthenium–selenium, $RuSe_x$ (Ru, 20; Se, 1 wt%), nanoparticles were dispersed in the form of Nafion-containing inks on glassy carbon electrodes to produce electrocatalytic interfaces reactive towards electroreduction of dioxygen in acid medium (0.5 mol dm^{-3} H_2SO_4). It was apparent from the rotating disk voltammetric experiments that the reduction of oxygen proceeded at WO_3-modified electrocatalyst at more than 100 mV more positive potential when compared to bare (WO_3-free) $RuSe_x$ system (that had been prepared under analogous conditions and deposited at the same loading of 156 μg cm^{-2}). The ring-disk rotating voltammetric measurements show that, while the production of hydrogen peroxide intermediate was significantly lower, the kinetic parameter (heterogeneous rate constant) for the oxygen reduction was higher for WO_3-modified $RuSe_x$ (relative to bare $RuSe_x$). Comparison was also made to highly-efficient Vulcan-supported Pt or Pt/Co nanoparticles: while the half-wave potential for the oxygen reduction at WO_3-modified carbon-supported $RuSe_x$ was still more negative relative to the potentials characteristic of Pt-based electrocatalysts, the oxygen reduction rotating disk voltammetric current densities (measured at 1600 rpm) were almost identical.

Keywords Oxygen reduction · Rotating disk voltammetry · Acid electrolyte · Ruthenium–selenium nanoparticles · Tungsten oxide

1 Introduction

Fuel cells are becoming an important subject of intense applied and fundamental research. The direct methanol fuel cells (DMFC) have recently attracted interest with respect to possible application as alternative power sources for portable electronic devices [1–4] and vehicles [2, 5]. One of the fundamental problems related to the operation of methanol–oxygen fuel cells is methanol crossover through the polymer membrane from the anode to the cathode compartment where it can be oxidized at potentials also suited for oxygen reduction. The co-existence of both reactions (the reduction of oxygen and the oxidation of methanol) leads to the concomitant depolarization of the platinum cathode. There is a need to search for highly reactive but methanol-tolerant (i.e. selective for the oxygen reduction reaction) electrocatalysts as potential electrode materials for DMFC cathodes.

Although platinum based electrocatalysts are still the most commonly used systems for the reduction of oxygen in acid media, there have been many attempts to synthesize different catalytic materials [3, 4, 6, 7]. Bi-component ruthenium–selenium ($RuSe_x$) nanoparticles can be viewed as a promising alternative to Pt and Pt-alloy based cathode

P. J. Kulesza (✉) · K. Miecznikowski · B. Baranowska · M. Skunik · A. Kolary-Zurowska · A. Lewera · K. Karnicka · M. Chojak · I. Rutkowska
Department of Chemistry, University of Warsaw, Pasteura 1, Warsaw 02-093, Poland
e-mail: pkulesza@chem.uw.edu.pl

S. Fiechter · P. Bogdanoff · I. Dorbandt · G. Zehl
Hahn-Meitner-Institut, Abt. Solare Energetic, Glienicker Str. 100, 14109 Berlin, Germany

R. Hiesgen · E. Dirk
Department of Basic Sciences, University of Applied Sciences Esslingen, Kanalstrasse 33, 73728 Esslingen, Germany

K. S. Nagabhushana · H. Boennemann
Forschungszentrum Karslruhe in der Helmholtz-Gemeinschaft Institut fur Technische Chemie ITC-CPV, Karslruhe, Germany

materials. Contrary to Pt type systems, the catalysts utilizing $RuSe_x$ have been reported to be fully methanol tolerant [8–17]. While bare Ru metal itself is a poor oxygen reduction catalyst, the addition of Se exhibits a profound activating effect. Although there is no unequivocal explanation of the phenomenon of enhancement, a reasonable possibility takes into account chemical stabilization of metallic Ru centers against oxidative degradation through "coordination" of Ru by Se atoms [17].

In terms of current densities, the reactivity of $RuSe_x$ is pretty high because the system is capable to drive the reduction of oxygen to water as the predominant final product, i.e. with the involvement of almost four electrons and with the formation of only small amounts of hydrogen peroxide intermediate (<5–6%) [15, 18–20, G. Zehl et al. (2006, submitted)]. On the other hand, to make the system competitive to Pt based catalysts, one would have to develop means of activating $RuSe_x$ catalytic centers to carry out the oxygen reduction reaction at effectively more positive potentials.

In our recent preliminary communication [22], we have reported that modification of carbon-supported $RuSe_x$ nanoparticles with ultra-thin films of tungsten oxide tends to shift the oxygen reduction potential towards more positive values. Historically, WO_3 was found to exhibit powerful catalytic properties towards electroreduction of hydrogen peroxide [23, 24]. In the present work, using rotating ring-disk electrode (RRDE) voltammetry, we address the problem of the formation of H_2O_2 intermediate at bare and WO_3-modified $RuSe_x$ when a moderate loading (ca. 156 μg cm^{-2}) of the binary electrocatalyst was electrodeposited on glassy carbon disk. The observed lower percent production of hydrogen peroxide, the positive shift of the half-wave potential and the increase in the kinetic parameter (heterogeneous rate constant) clearly imply that modification of $RuSe_x$ with WO_3 films results in enhancement of the electrocatalytic properties towards electroreduction of oxygen in acid medium (0.5 mol dm^{-3} H_2SO_4). Finally, the activity of the WO_3-modified $RuSe_x$ has also been compared to the performance of well-established Vulcan-supported Pt and Pt/Co electrocatalysts for the oxygen reduction.

2 Experimental

The electrochemical experiments were performed with CH Instruments (Austin, TX, USA) Model 750A workstation. A mercury/mercury sulfate electrode (Hg/Hg_2SO_4), the potential of which was 640 mV more positive relative to the reversible hydrogen electrode (RHE), was used as a reference electrode. This electrode was placed in the second compartment and connected to the main cell through a Lugging capillary. All potentials are expressed against the RHE.

Rotating disk electrode (RDE) and RRDE voltammetric measurements were accomplished using a variable speed rotator (Pine Instruments, USA). The electrode assembly utilized a glassy carbon disk and a Pt ring. The electrodes were polished with successively finer grade aqueous alumina slurries (grain size, 5-0.05 μm) on a Buehler polishing cloth. In the RRDE measurements, the radius of the disk electrode was 2.3 mm, and the inner and outer radii of the ring electrode were 2.46 and 2.7 mm, respectively. The collection efficiency of the RRDE assembly was determined from the ratio of ring and disk currents (at various rotation rates) using the argon-saturated 0.005 mol dm^{-3} $K_3[Fe(CN)_6]$ + 0.01 mol dm^{-3} K_2SO_4 solution [G. Zehl et al. (2006, submitted), 25]. Based on five independent experiments, it was found that, within the potential range considered here, and at rotation rates up to 2500 rpm, the experimental collection efficiency (N) remained unchanged and was equal to 0.23. During the RRDE measurements in oxygen saturated solutions, the potential of the ring electrode was kept at 1.2 V. At this potential, the generated H_2O_2 is readily oxidized under diffusional-convective control. All RDE and RRDE polarization curves were recorded at a scan rate of 10 mV s^{-1}.

All chemicals were commercial materials of the highest available purity (ACS reagent grade) and were used as received. Solutions were prepared from triply distilled subsequently deionized water. They were deaerated (using prepurified argon) or saturated with oxygen for at least 10 min prior to the electrochemical experiment. Experiments were conducted at room temperature (20 ± 0.5 °C).

Carbon (Vulcan) supported $RuSe_x$ ($RuSe_x$/C) clusters were fabricated at HMI, Berlin, using the procedure analogous to that described earlier [G. Zehl et al. (2006, submitted)]. In brief, a commercially available Vulcan (XC72) supported Ru (20 wt%) catalyst from ETEK was modified with selenium by its impregnation with an acetonic solution of selenium tetrachloride ($SeCl_4$) followed by reductive annealing under forming gas. Their composition of the final material was as follows: Ru, 20; Se, 1; and C 79% (by mass). The diameters of carbon supports and $RuSe_x$ particles were approximately 20 and 2 nm, respectively. To produce a suspension of bare $RuSe_x$/C nanoparticles, a known amount (25 mg) of the catalyst was dispersed in 2 cm^3 of water and subjected to sonication for 10 min. The suspension of WO_3-modified $RuSe_x$/C was produced as follows. A known amount (25 mg) of $RuSe_x$/C was dispersed in 2 cm^3 solution of tungstic acid (that had been obtained by passing an aqueous 0.1 mol dm^{-3} Na_2WO_4 solution through a proton exchange resin, Dowex 50 WX2-200). Formation of ultra-thin WO_3 films on $RuSe_x$/C occurred through the sol–gel aggregation aging

process. As a rule, 10 μdm^3 aliquot of the appropriate suspension was dropped onto the surface of a glassy carbon disk electrode (geometric area, 0.16 cm^2), and the suspension was air-dried at room temperature. The catalyst layer (bare or modified with WO_3) was subsequently overcoated with Nafion film by adding 3 μdm^3 of the ethanolic Nafion solution (from Aldrich). As a rule the catalytic films were activated by performing 20–30 full voltammetric potential cycles in the potential range from 0 V to 0.9 V (at 50 mV s^{-1}) until steady-state currents were observed. While the morphology of catalytic films was examined using scanning electron microscopy (SEM), the bare and WO_3-modified carbon (Vulcan)-supported $RuSe_x$ nanoparticles were first monitored using Philips CM 10 transmission electron microscopy (TEM) operating at 100 kV.

Nanoparticles of carbon (Vulcan XC-72) supported platinum (from ZSW, Ulm Germany) and of carbon (Black Pearl) supported platinum–cobalt (Pt_3Co) alloy (from Forschungszentrum Karslruhe, Germany), with the relative metal loadings on the level 40 wt%, were used as comparative catalysts for the oxygen electroreduction. According to the manufacturers' information, the sizes of Pt and Pt_3Co particles were approximately 2–3 nm. They were deposited on glassy carbon disks in a manner analogous to that described for $RuSe_x$/C nanoparticles.

3 Results and discussion

Typical TEM images of carbon-supported $RuSe_x$ nanoparticles $RuSe_x$/C, (A) bare and (B) modified with ultrathin layers of tungsten oxide, are illustrated in Fig. 1. The dark dots represent $RuSe_x$ nanoparticles (Fig. 1A). They have diameters ranging from 2 nm to 3 nm (for brevity, a TEM with larger magnification is not shown here). The lighter areas in Fig. 1A should be attributed to relatively larger (bulk) carbon (Vulcan) supports; they are approximately spherical and tend to form agglomerates (Fig. 1A). But the grayish portions (existing within the lighter areas of Fig. 1B) should reflect the presence of metal oxide (WO_3) structures in addition to carbon supports. Tungsten oxides seem to be amorphous or polycrystalline, and they overcoat the $RuSe_x$/C agglomerates of Fig. 1A. Thickness of WO_3 overlayers is roughly on the level of tens of nm, and it exceeds the size of $RuSe_x$ nanoparticles.

Figure 2 shows SEM images of $RuSe_x$/C nanoparticles, (A) bare and (B) modified tungsten oxide, following deposition in a form of Nafion-containing inks on glassy carbon substrates. In both cases, the catalytic particles form agglomerates on a micrometer scale. But morphology of the WO_3-modifed system (Fig. 2B) seems to be much denser when compared to WO_3-free material (Fig. 2A). It is likely that tungsten oxide and/or the mixed Nafion/oxide

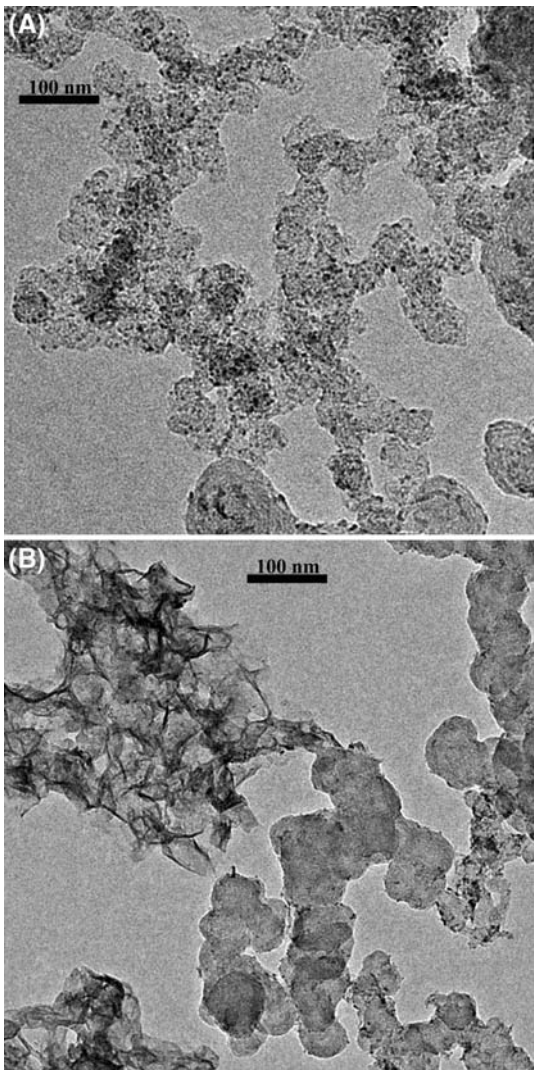

Fig. 1 Transmission electron micrographs of (**A**) bare and (**B**) WO_3-modified $RuSe_x$/C nanoparticles. While the dark dots represent $RuSe_x$ nanoparticles, the grayish and light areas stand for carbon supports and tungsten oxide structures, respectively

deposits are filling the void spaces between the $RuSe_x$/C nanoparticles.

Figure 3 shows cyclic voltammetric responses of (A) bare, and (B) and WO_3-modified $RuSe_x$/C nanoparticles deposited on glassy carbon electrode and investigated in the deaerated 0.5 mol dm^{-3} H_2SO_4 solution. The main differences between cyclic voltammograms of bare and WO_3-modified $RuSe_x$/C catalysts are as follows. While the bare $RuSe_x$/C catalyst is characterized by a fairly flat background response (Fig. 3A), the latter system shows much higher voltammetric currents, particularly below 0.4 V (Fig. 3B), originating from the existence of WO_3 overlayers. Indeed, tungsten oxides undergo reversible reduction to non-stoichiometric oxides, such as substoichiometric hydrogen tungsten oxide bronzes (H_xWO_3,

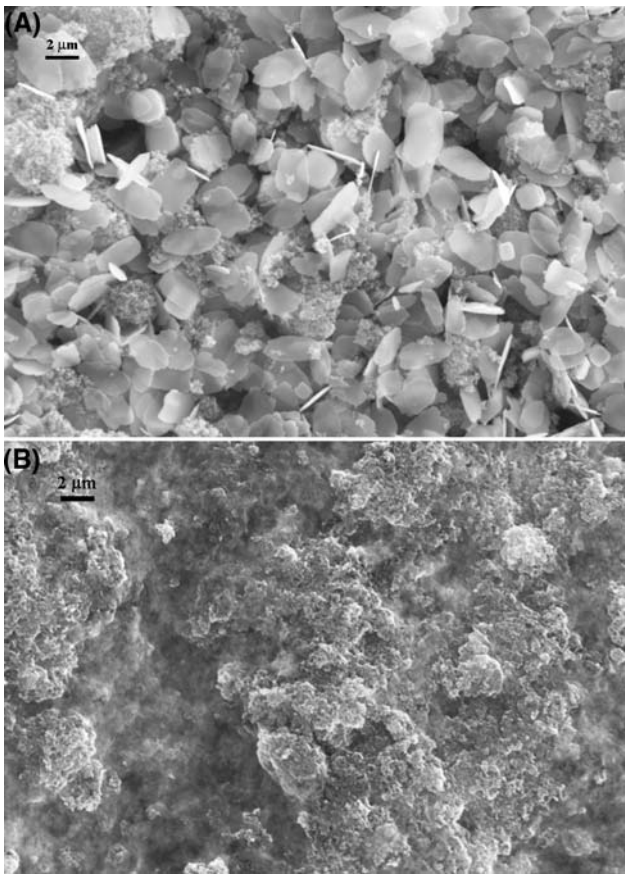

Fig. 2 Scanning electron micrographs of Nafion-treated inks of (**A**) bare and (**B**) WO_3-modified $RuSe_x$/C nanoparticles deposited on glassy carbon substrate

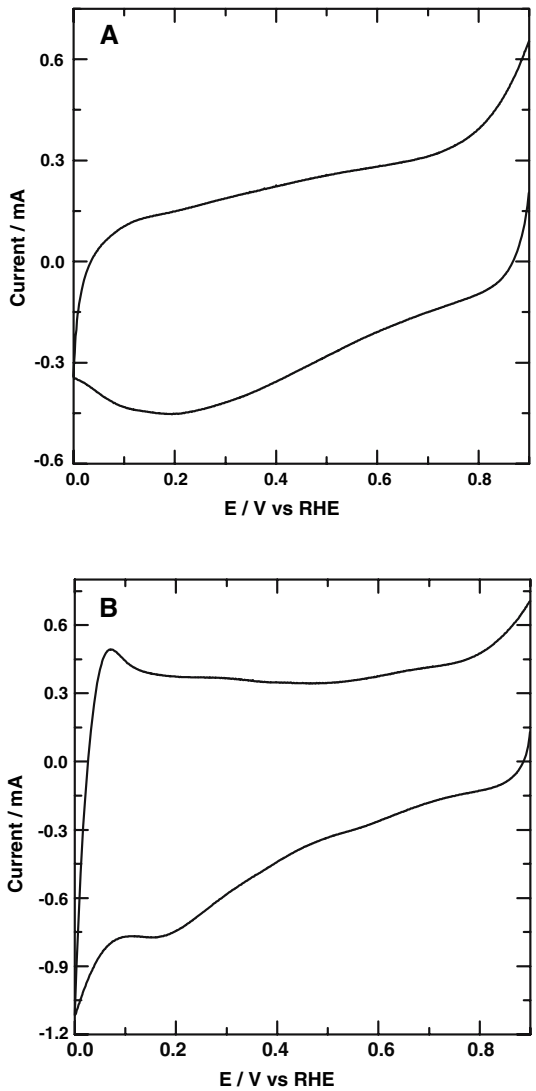

Fig. 3 Comparison of cyclic voltammetric responses of Nafion-treated inks of (**A**) bare and (**B**) WO_3-modified $RuSe_x$/C nanoparticles deposited on glassy carbon. Scan rate: 50 mV s^{-1}. Electrolyte: 0.5 mol dm^{-3} H_2SO_4

$0 < x < 1$) or lower tungsten oxides (WO_{3-y}, $0 < y < 1$) [23, 24] at potentials mentioned above. Finally, the current increases at potentials higher than 0.75 V observed for both bare and WO_3-modified $RuSe_x$/C catalysts (Fig. 3A, B) most likely reflect some oxidation of the Se-covered metallic Ru nanoparticles.

Rotating ring-disk electrode voltammetry was used to study the electrocatalytic properties of the Nafion-treated inks (deposited on glassy carbon disks) of $RuSe_x$/C nanoparticles towards the oxygen reduction reaction in the O_2-saturated 0.5 mol dm^{-3} H_2SO_4 solution (Fig. 4). While current – potential Curves **a** and **b** describe disk responses for WO_3-free and WO_3-modified catalytic nanoparticles, the Curves **a′** and **b′** refer to the respective ring responses. The results are consistent with the view that the modification of $RuSe_x$/C nanoparticles with ultra-thin films of tungsten oxide shifts the half-wave potential of the RDE oxygen reduction voltammogram (Curve **b**) ca. 100 mV towards more positive values when compared to the potential characteristic of the bare $RuSe_x$/C nanoparticles (Curve **a**). This potential effect is almost perfectly reproducible within ±5 mV. Based on numerous experiments done on various samples, the disk currents, when measured at 0.2 V upon application 1600 rpm rotation rate, are reproducible within 5%. The value of disk current density determined for the WO_3-modified system (Curve **b**) has been found to be statistically only slightly higher in comparison to the system utilizing bare catalytic nanoparticles (Curve **a**). But ring currents differ much more significantly, clearly implying much more pronounced formation of hydrogen peroxide intermediate (particularly at potentials lower than 0.5 V) in the case of the system containing bare $RuSe_x$/C nanoparticles (Curve **a′**) relative to the system with WO_3-modified ones (Curve **b′**). It is apparent from the comparison of the data of Figs. 3B and 4 (Curve **b′**) that the relative decrease of the hydrogen peroxide formation starts to occur at potentials where tungsten oxide is

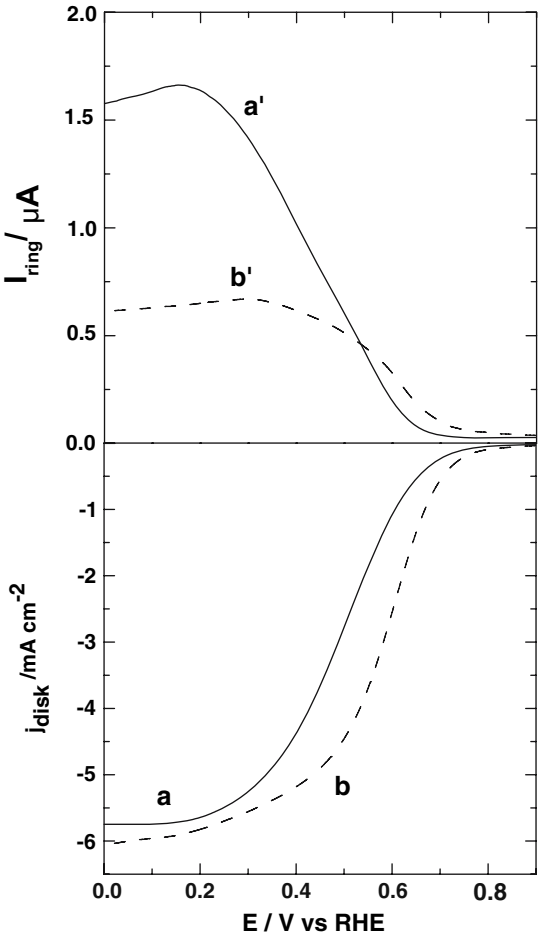

Fig. 4 RRDE voltammetric diagnostic experiments performed in 0.5 mol dm^{-3} H_2SO_4, at 1600 rpm, and at 10 mV s^{-1} scan rate. While **a** and **b** refer to disk current-potential curves, the ring (Pt) responses are marked as **a′** and **b′** for the measurements done at catalytic layers (deposited on glassy carbon disks) containing bare and WO_3-modified $RuSe_x$/C nanoparticles, respectively. Ring potential, 1.2 V

becoming electroactive, namely where it is reduced to hydrogen bronzes (that are known to be catalytic towards reduction of H_2O_2 [24]). This result implies direct involvement of tungsten oxide overlays (on $RuSe_x$/C) in the oxygen electroreduction reaction. It should be remembered that partially reduced tungsten oxides should also act as good mediators facilitating electron transfers to dispersed $RuSe_x$ sites. Further, the mixed deposits of WO_3 and Nafion presumably serve as sources of interfacial mobile protons (improved H^+ mobility) that are necessary to support the four-electron reduction of oxygen to water. The latter phenomena may also explain the positive shift in the potential for the electroreduction of oxygen in the system containing WO_3 (compare Curves **a** and **b** in Fig. 4).

To obtain more quantitative information about the relative formation of hydrogen peroxide during RRDE measurements at glassy carbon disk electrodes covered with bare and WO_3-modified $RuSe_x$ catalytic centers, the % amounts of H_2O_2 ($X_{\%H_2O_2}$) have been calculated from the data of Fig. 4 by using the following relationship [G. Zehl et al. (2006, submitted), 25]:

$$X_{\%H2O2} = (200I_r/N)/(I_d/(I_r/N)) \quad (1)$$

where I_r is ring current, I_d stands for disk current, and N is the collection efficiency. The approach is based on the assumption that oxygen undergoes reduction according to two parallel mechanisms: 4-electron reaction to water and 2-electron to hydrogen peroxide. Typical results of calculations are displayed in Fig. 5. In the case of both bare and WO_3-modified $RuSe_x$ nanoparticles, the production of H_2O_2 is sizeable at potentials higher than 0.6 V. Under such conditions, the oxygen reduction RDE currents are not well developed yet (refer to Curves **a** and **b** in Fig. 4) because the potentials are not sufficiently negative to effectively drive the oxygen reduction reaction. Nevertheless, the relative formation of hydrogen peroxide is much higher at the catalyst containing WO_3-free (bare) $RuSe_x$/C. At potentials not exceeding 0.6 V, the values of ($X_{\%H_2O_2}$) are fairly low, as apparent from Fig. 5, and they are below 2 and 1% for the systems utilizing bare (Curve **a**) and WO_3-modified (Curve **b**) catalytic $RuSe_x$/C nanoparticles. On the whole, the data of Fig. 5 are consistent with the view that, in the all potential ranges considered here, the relative formation of hydrogen peroxide is lower in the presence of tungsten oxide.

The representative RDE voltammograms recorded at different rotation rates (ranging from 200 rpm to 2500 rpm) for the oxygen reduction at catalytic layers containing (A) WO_3-free and (B) WO_3-modified $RuSe_x$/C

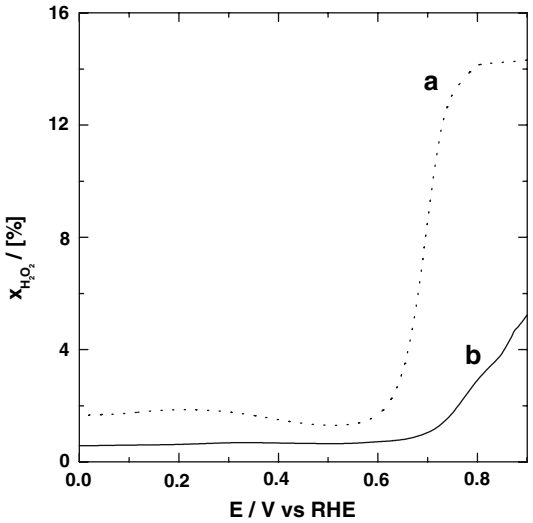

Fig. 5 Fraction of hydrogen peroxide ($X_{H_2O_2}$) produced during electroreduction of oxygen under the condition of RRDE voltammetric experiment of Fig. 4

nanoparticles are illustrated in Fig. 6. In both cases, the RDE responses are fairly well-defined at any rotation rate studied. Further, half-wave potentials for the reduction of oxygen at the system containing WO_3-modified $RuSe_x$/C (Fig. 6B) are shifted at least 100 mV in the positive direction when compared to those characteristic of the WO_3-free system (Fig. 6A). The voltammograms of Fig. 6 have been analyzed by the usual means. When the dependencies (Levich type plots) of the RDE current densities (measured at 0.45 V) is plotted versus square root of rotation rates) for electrodes covered with (a) WO_3-free and (b) WO_3-modified $RuSe_x$/C (Insets to Fig. 5a, b), respectively, deviation from linearity (i.e. from the ideal

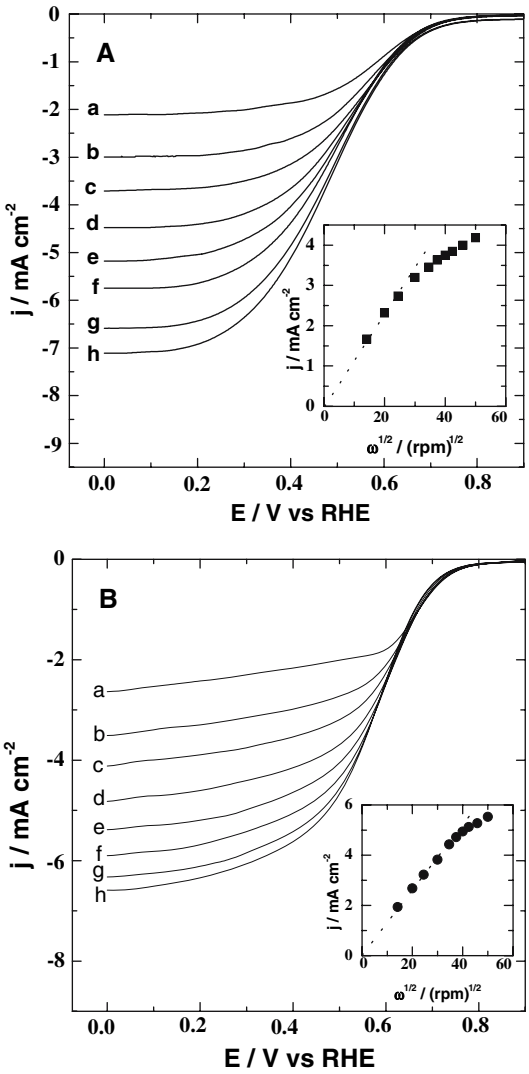

Fig. 6 RDE voltammograms for the oxygen reduction at catalytic layers (deposited on glassy carbon disks) containing (**A**) bare and (**B**) WO_3-modified $RuSe_x$/C nanoparticles. The respective Levich plots of current densities versus square root of rotation rate ($\omega^{1/2}$) for the electroreduction of oxygen (at 0. 45 V) are shown in Insets. Rotation rates: (a) 200, (b) 400, (c) 600, (d) 900, (e) 1200, (f) 1600, (g) 2100, and (h) 2500 rpm. Other conditions as for Fig. 4

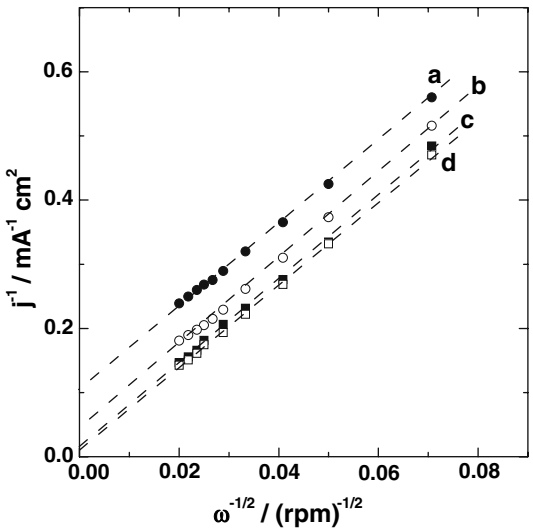

Fig. 7 Koutecky-Levich reciprocal plots (prepared using the data of Fig. 6) for the electroreduction of oxygen (at 0. 45 V) at catalytic layers (deposited on glassy carbon disks) containing (**a**) bare and (**b**) WO_3-modified $RuSe_x$/C nanoparticles. For comparison, the analogous plots are provided for (**c**) Vulcan supported Pt nanoparticles (40 wt%) and (**d**) Vulcan supported Pt/Co nanoparticles. In all cases, the loadings of metallic (bimetallic) catalysts were approximately 150 μg cm^{-2}

behavior characteristic of systems limited solely by convective diffusion of oxygen in solution) is observed, and seems to be more pronounced at bare rather than WO_3-modified system. Apparently, the kinetic control is more pronounced, i.e. the catalytic reaction is slower (or less effective) in the case of bare $RuSe_x$/C nanoparticles. We have further analyzed the results by means of so called Koutecky-Levich reciprocal plots [24, 25, 27]. Such diagnosis (Fig. 7) is justified because charge (electron, proton) propagation within the catalytic film should be fast, and the oxygen reactant is expected to have easy access to the dispersed active sites (bare or WO_3-modified $RuSe_x$/C nanoparticles). With low amounts of Nafion added to form the inks, any possible limitations related to mass transport through mixed WO_3-Nafion layers (which may affect the measured current densities) will be considered relatively negligible. We assume that only such factors as transport of oxygen in solution or, at higher rotation rates, the dynamics of the chemical (catalytic) step (reaction) are rate determining. The reciprocal plots (Curves **a** and **b** in Fig. 7) have yielded non-zero intercepts clearly indicating kinetic limitations associated with the electrocatalytic film.

The RDE voltammetric limiting-current densities (j_{lim}) can be expressed as follows [24, 25]:

$$j_{lim}^{-1} = \left(nFkC_{film}C_{Ox}\right)^{-1} + j_L^{-1} \quad (2)$$

where j_L is given by the Levich equation (in which the convective diffusion component is proportional to square

root of rotation rate), k is the rate constant for the catalytic reaction in homogeneous units, C_{film} is the surface concentration of the electrocatalyst, and C_{Ox} is the bulk concentration of oxygen (1.1 mmol dm^{-3} [26]). The symbols n and F stand for the number of electrons involved in the process (n = 4) and the Faraday constant. The kinetic parameters can be found from intercepts of the reciprocal plots (Fig. 7). The estimated value of kC_{film}, which is equivalent to the intrinsic rate of heterogeneous charge transfer, is 7×10^{-2} cm s^{-1} for the catalytic electroreduction (at 0.45 V) of oxygen at glassy carbon disks covered with WO_3-modified $RuSe_x$/C nanoparticles (Fig. 7, Curve **b**). When we performed the analogous determination for bare $RuSe_x$/C (Fig. 7, Curve **a**), the heterogeneous rate constant was found to be 2×10^{-2} cm s^{-1}. The above results are reproducible within 5–10% in different experiments. The data simply imply that modification of $RuSe_x$/C with ultra-thin layers of WO_3 to the ink results in statistically some (more than three times) increase in the heterogeneous rate constant for oxygen reduction.

Finally, we compared the electrocatalytic performance of WO_3-modified $RuSe_x$/C to the behavior of carbon (Vulcan) supported Pt nanoparticles and carbon (Black Pearl) supported Pt/Co (namely Pt_3Co) bimetallic nanoparticles deposited on glassy carbon in the form of inks prepared in the analogous manner to those containing $RuSe_x$/C. Figure 8 shows the respective RDE voltammograms recorded at 1600 rpm. Although the limiting currents are comparable in all three cases, the half-wave potentials for the electroreduction of oxygen are still ca. 180 or 230 mV more negative in the case of WO_3-modified $RuSe_x$/C (Fig. 8, Curve **a**) when compared to the behavior at Pt (Fig. 8, Curve **b**) or Pt/Co (Fig. 8, Curve **c**). When the kC_{film} parameters (for the electroreduction of oxygen) were estimated from the intercepts of Koutecky-Levich plots (at 0.6 V) for Vulcan-supported Pt (Fig. 7, curve **c**) and Black Pearl supported Pt/Co (Fig. 7, curve **d**) nanoparticles (deposited on glassy carbon disks), the following values, 2×10^{-1} and 3×10^{-1} cm s^{-1} were obtained, respectively. These values are obviously somewhat higher than those determined by us for WO_3-modified $RuSe_x$/C.

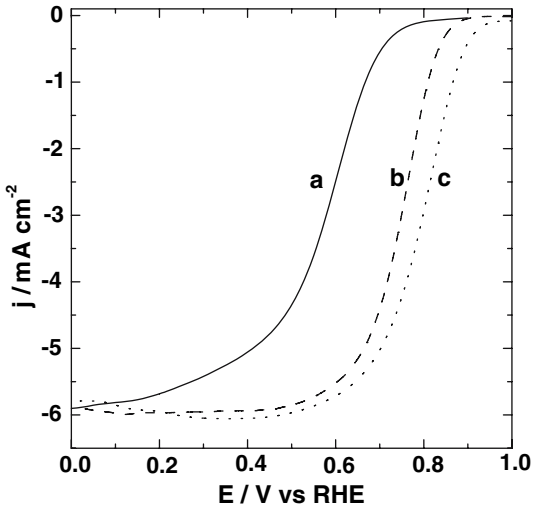

Fig. 8 RDE voltammetric diagnostic (comparative) measurements performed in 0.5 mol dm^{-3} H_2SO_4, at 1600 rpm, and at 10 mV s^{-1} scan rate. Curves **a**, **b**, and **c** refer to current-potential responses obtained at catalytic layers (deposited on glassy carbon disks) of WO_3-modified $RuSe_x$/C, Vulcan supported Pt (40 wt%), and Vulcan supported Pt/Co nanoparticles

In conclusion, the performance of our WO_3-modified $RuSe_x$/C electrocatalyst is lower, in comparison to Pt-based systems, and further research is necessary to find means of further activation of $RuSe_x$ nanoparticles to shift the oxygen reduction potential towards more positive values. On the other hand, the results clearly show that, by application of such reactive (towards hydrogen peroxide) and protonically/electronically conducting matrix as tungsten oxide [22–24, 28], some enhancement of the oxygen electroreduction at $RuSe_x$/C is feasible. There are still possibilities to manipulate the WO_3 thickness and its morphology, as well as to utilize $RuSe_x$ nanoparticles of different compositions. The related results will be a subject of a future publication.

Acknowledgements This work was supported by the Network Efficient Oxygen Reduction for Electrochemical Energy Conversion (coordinated by ZSW, Ulm, Germany). The Warsaw group acknowledges partial support from Ministry of Science and Higher Education (Poland) under the grant N204 164 32/4284. Helpful discussions with Prof. H. Tributsch of Hahn-Meitner-Institut, Berlin are appreciated.

References

1. Kordesch K, Simader G (1996) Fuel cells and their applications. Wiley-VCH, Weinheim
2. Wasmus S, Kuver A (1999) J Electroanal Chem 461:14
3. Arico AS, Srinivasan S, Antonucci V (2001) Fuel Cells 1:133
4. Hogarth MP, Hards GA (1996) Platinum Met Rev 40:150
5. Vielstich W, Lamm A, Gasteiger H (eds) (2003) Handbook of fuel cells; A., vol 2. Wiley, Chichester
6. Chu D, Gilman S (1994) J Electrochem Soc 141:177
7. Heinzel A, Barragan VM (1999) J Power Sources 84:70
8. Alonso-Vante N, Bogdanoff P, Tributsch H (2000) J Catal 190:240
9. Holze R, Vogel I, Vielstich W (1986) J Electroanal Chem Interfacial Electrochem 210:277
10. Bittins-Cattaneo B, Wasmus S, Lopez-Mishima B, Vielstich W (1993) J Appl Electrochem 23:625
11. Rodriguez FJ, Sebastian PJ, Solorza O (1998) Int J Hydrogen Energy 23:1031
12. Tributsch H, Bron M, Hilgendorff M, Schulenburg H, Dorbandt I, Eyert V, Bogdanoff P, Fiechter S (2001) J Appl Electrochem 31:739
13. Chu D, Jiang R (2002) Solid State Ionics 148:591
14. Solorza-Feria O, Ellmer K, Giersig M, Alonso-Vante N (1994) Electrochim Acta 39:1647

15. Schmidt TJ, Paulus UA, Gasteiger HA, Alonso-Vante N, Behm RJ (2000) J Electrochem Soc 147:2620
16. Malakhov IV, Nikitenko SG, Savinova ER, Kochubey DI, Alonso-Vante N (2002) J Phys Chem B 106:1670
17. Cao D, Wieckowski A, Inukai J, Alonso-Vante N (2006) J Electrochem Soc 153:A874
18. Alonso-Vante N, Solorza-Feria O (1995) Electrochim Acta 40:567
19. Paulus UA, Schmidt TJ, Gasteiger HA, Behm RJ (2001) J Electroanal Chem 495:134
20. Schulenburg H, Hilgendorff M, Dorbandt I, Radnik J, Peter Bogdanoff S, Fiechter M, Bron H, Tributsch J (2006) Power Sources 155:47
21. Zaikovskii VI, Nagabhushana KS, Kriventsov VV, Loponov KN, Cherepanova SV, Kvon RI, Bonnemann H, Kochubey DI, Savinova ER (2006) J Phys Chem B 110:6881
22. Kulesza PJ, Miecznikowski K, Baranowska B, Skutnik M, Fiechter S, Bogdanoff P, Dorbandt I (2006) Electrochem Comm 8:904
23. Kulesza PJ, Faulkner LR (1988) J Electroanal Chem 248:305
24. Kulesza PJ, Grzybowska B, Malik MA, Galkowski MT (1997) J Electrochem Soc 144:1911
25. Stamenkovic V, Schmidt TJ, Ross PN, Markovic NM (2003) J Electroanal Chem 554–555:191
26. Zecevic SK, Wainright JS, Litt MH, Gojkovic SLj, Savinell RF (1997) J Electrochem Soc 144:2973
27. Paulus UA, Schmidt TJ, Gsteiger HA, Behm RJ (2001) J Electroanal Chem 495:134
28. Colmenares L, Jusys Z, Kinge S, Boennemann H, Behm RJ (2006) J New Mater Electrochem Syst 9:107